Electronic Supplementary Material (ESI) for Journal of Materials Chemistry A.
This journal is © The Royal Society of Chemistry 2021

Supplementary information

Precursor solution dependent secondary phase defects in $CsPbBr_3$ single crystal grown by inverse temperature crystallization

Yuanbo Cheng,[†, ‡] Menghua Zhu,[†] Fangbao Wang,[†] Ruichen Bai,[†] Jinshan Yao,[‡] Wanqi Jie,[†] and Yadong Xu[,†]*

[†]State Key Laboratory of Solidification Processing, and Key Laboratory of Radiation Detection Materials and Devices, Northwestern Polytechnical University, Xi'an 710072, China.

[‡]National Laboratory of Solid State Microstructures & Department of Materials Science and Engineering, College of Engineering and Applied Sciences, Nanjing University, Nanjing 210093, China.

Corresponding Author

*Tel: +86-29-88460445; E-mail address: xyd220@nwpu.edu.cn (Y. Xu)

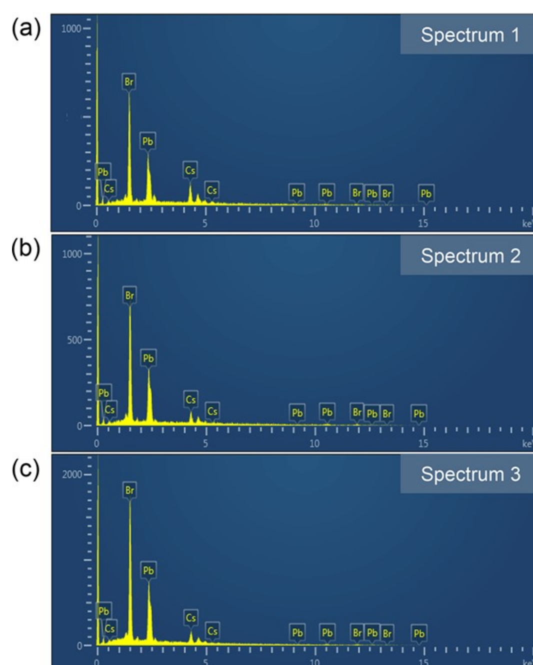

Fig. S1 EDS scanning counting spectrum of different elements, (a) point 1, (b) point 2, and (c) point 3.

Table S1 Contents of elements at different points tested by EDS micro area

Element	#1		#2		#3	
—	at. %	ratio	at. %	Ratio	at. %	ratio
Cs	11.76	0.99	12.45	0.97	18.68	0.96
Pb	23.64	2.00	25.59	2.00	19.43	1.00
Br	64.60	5.46	61.97	4.84	61.89	3.18
Total	100	$CsPb_2Br_5$	100	$CsPb_2Br_5$	100	$CsPbBr_3$

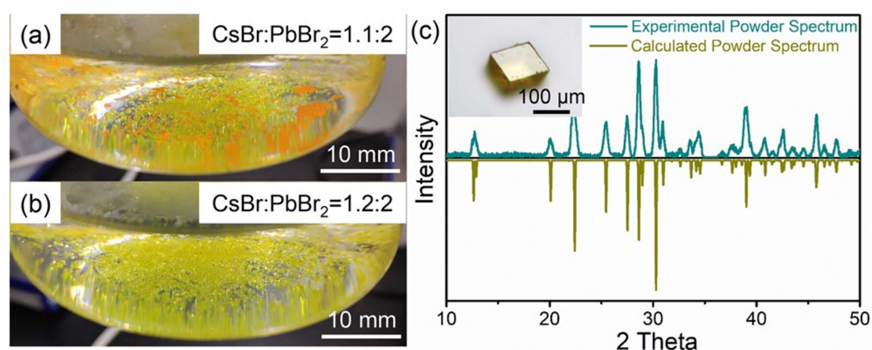

Fig. S2 Crystals precipitated from precursor solution with different raw material ratios. (a) $CsBr:PbBr_2$=1.1:2, and (b) $CsBr:PbBr_2$=1.2:2. (c) Powder X-ray diffraction (PXRD) pattern of precipitated crystal, the inset is typical optical microscope image of micron-scale crystal.

The light yellow micron-scale optically clear crystals mixed with orange grains precipitate at the bottom of the precursor solution with an intermediate CsBr:$PbBr_2$ ratios of 1.1 : 2 (Fig. S2a). The rhombohedral crystal is observed by optical microscope, as shown in the inset of Fig. S2c. Powder XRD pattern shows that the precipitated lightly yellow crystal is Cs_4PbBr_6. With the precursor solution ratio increases to CsBr:$PbBr_2$=1.2 : 2, pure Cs_4PbBr_6 precipitates at the preset temperature (Fig. S2b).

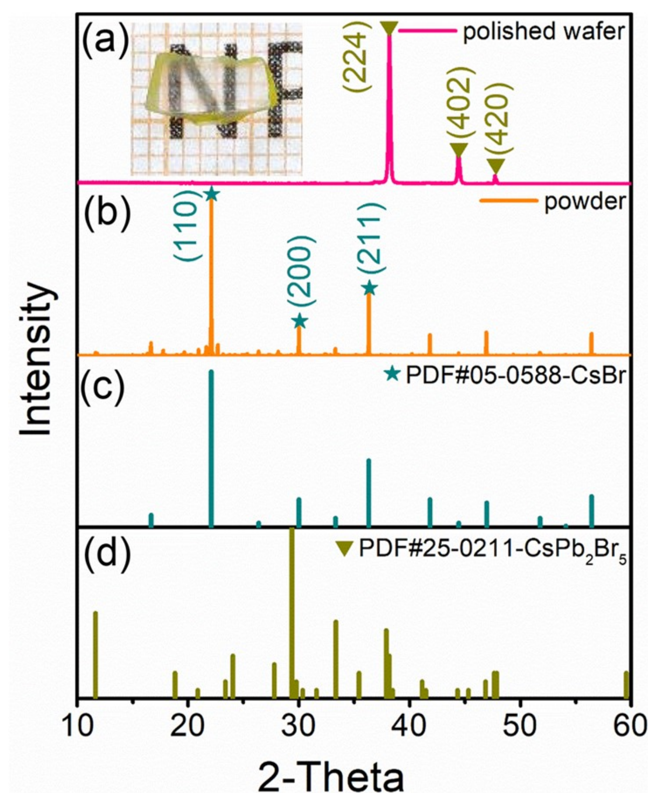

Fig. S3 (a) XRD pattern of the polishing transparent block, and the inset is the typical image of optical microscope. (b) Powder XRD pattern. (c) PDF card #05-0588 of CsBr. (d) PDF card #25-0211 of $CsPb_2Br_5$.

Repeat the synthesis steps, a little white block residue is observed at the bottom of beaker with the calculation ratio of CsBr : $PbBr_2$=1 : 2. The PXRD spectrum shows that the block is mainly composed of CsBr, with a few diffraction peaks of $CsPb_2Br_5$ (Fig. S3b). Moreover, the diffraction peak of $CsPb_2Br_5$ is detected on the polished wafer surface (Fig. S3a), which indicated that the transparent block is CsBr with a

small amount of adhered $CsPb_2Br_5$. It demonstrates that the slightly deviation of pristine materials ratio CsBr : $PbBr_2$=1:2 will lead to the secondary phase (SP) defects.

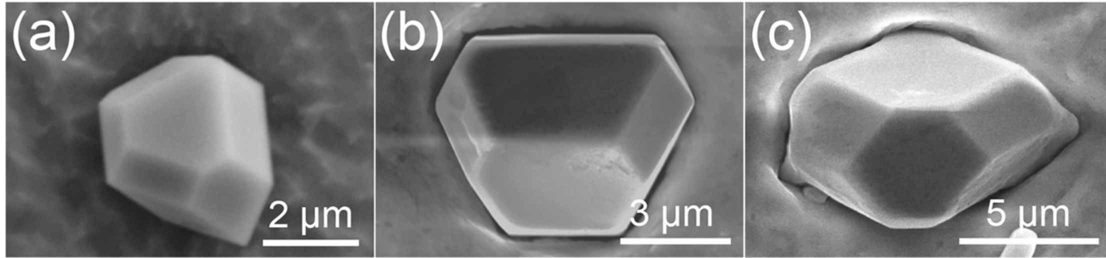

Fig. S4 (a)-(c) Three typical SEM morphology of "twisted crystal" SP particles. These grain surfaces are usually composed of trapezoidal and pentagonal planes with low symmetry.

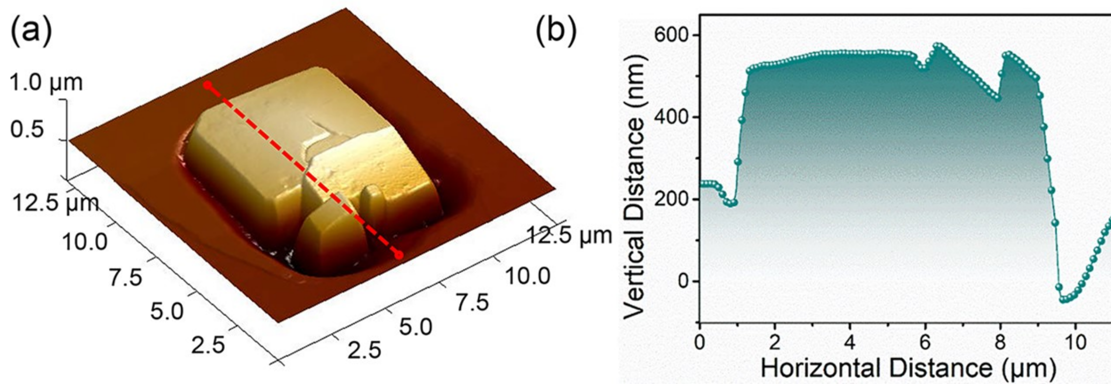

Fig. S5 (a) AFM images of SP particles on the surface of untreated $CsPbBr_3$ wafer. (b) Variation of wafer surface height along the direction of red dotted line.

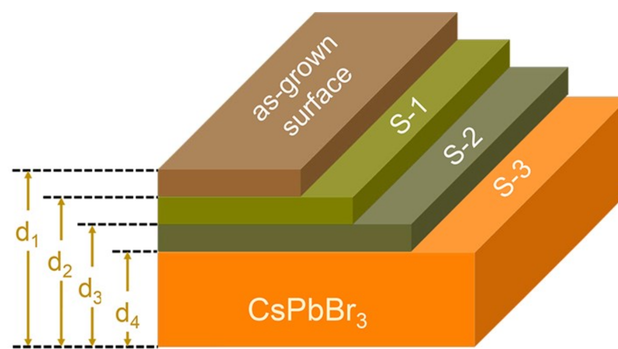

Fig. S6 Illustration of the $CsPbBr_3$ wafer thinning from top to bottom along the vertical growth direction. Different SP defects density surfaces color-coded differently.

Table S2 Thickness of $CsPbBr_3$ wafer thinned to different surface

Position	as-grown surface	S-1	S-2	S-3

Depth /mm	1.91	1.54	1.42	1.33

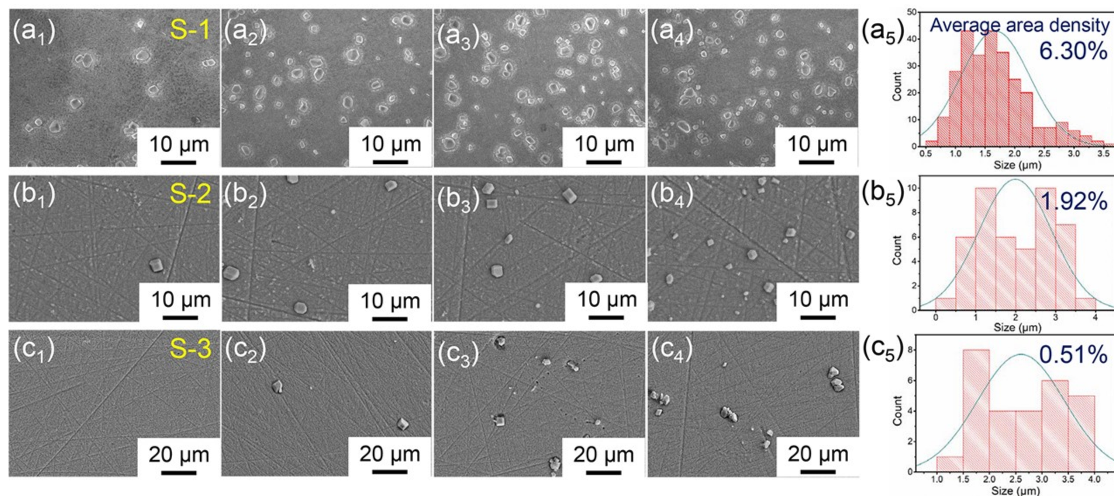

Fig. S7 The typical SEM images of SP defects distribution at different thickness wafer surfaces, with subscript marks 1, 2, 3 and 4 representing low, medium low, medium high and high density, and the subscript 5 corresponding to the size distribution histograms of SP defects at different surfaces, respectively, (a) S-1, (b) S-2 and (c) S-3. The number in the upper right corner is the estimated average area density of SP defects.

With the defect visualization processing, the observed distribution area density and size of SP defects at different thickness wafer surfaces show distinguishable. In S-1 wafer with smaller thinning thickness, there are more SP defects and the size is Gaussian distribution in the range of 0.5-3.5 μm. The number of SP defects in S-2 significantly reduce after further thinning of 0.1mm, and the SP defects are observed only in a few areas with the consistent particle size of S-1. As the thinning continues for another 0.1mm, SP defects is hard to be observed as shown in S-3, and most of the areas are SP-free.

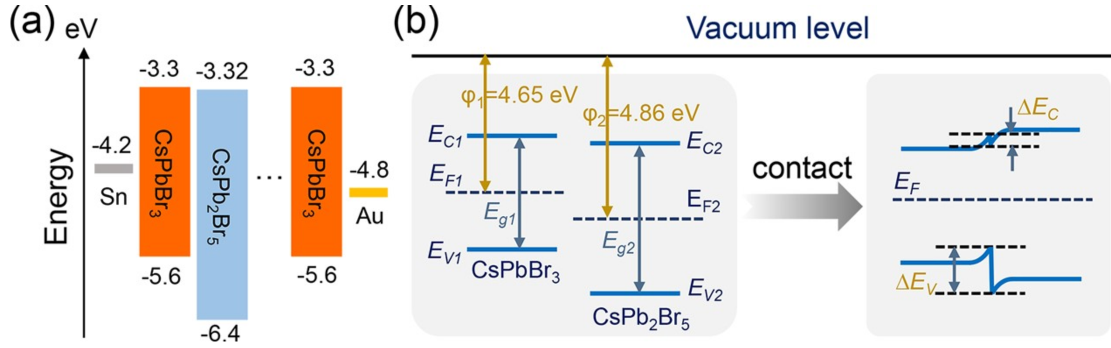

Fig. S8 Diagrams of energy band structures. (a) Schematic architecture of Au/$CsPbBr_3$/Sn device with corresponding energy band diagrams. (b) Before the contact of $CsPb_2Br_5$ and $CsPbBr_3$, and the formation of type I heterojunction after the two contact. E_C is the conduction band minimum, E_V is the valence band maximum, and E_F is the Fermi level.

The calculated work functions for $CsPb_2Br_5$ and $CsPbBr_3$ are 4.86 and 4.65 eV, and the band gap are 3.08 and 2.3 eV, respectively.[1-3] Barrier peaks and potential traps are induced by the discontinuous energy bands at the contact interface.

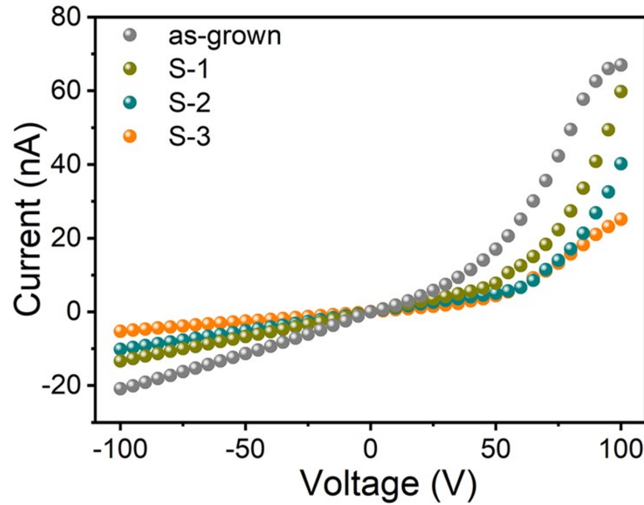

Fig. S9 Typical I–V characteristic curves of the Au/$CsPbBr_3$/Sn asymmetric electrode device at the range of ±100 V. The leakage current under positive and negative bias is improved after thinning.

References

1. Z. Yu, Y. Zhao, Q. Wan, B. Liu, J. Yang and M. Cai, *The Journal of Physical Chemistry C*, 2020, **124**, 23052-23058.
2. Z. Zhang, Y. Zhu, W. Wang, W. Zheng, R. Lin and F. Huang, *Journal of Materials Chemistry C*, 2018, **6**, 446-451.
3. Z. Huang, B. Ma, H. Wang, N. Li, R. Liu, Z. Zhang, X. Zhang, J. Zhao, P. Zheng and Q. Wang, *The Journal of Physical Chemistry Letters*, 2020, **11**, 6007-6015.